Modal analysis and condition monitoring for an electric motor through MEMS accelerometers

G. Mottola, P. Grosso, C. Fonte, M. Strozzi, R. Rubini, M. Cocconcelli [1]
[1] University of Modena and Reggio Emilia, Department of Sciences and Methods for Engineering
Via G. Amendola 2, 42122, Reggio Emilia, Italy
e-mail: **giovanni.mottola@unimore.it**

Abstract
Piezoelectric accelerometers are commonly employed for diagnosing machine faults, due to their accuracy. In the last few years, however, MEMS (Micro Electro-Mechanical Systems) accelerometers have attracted strong interest thanks to their low cost. In this work, a synchronous electric motor with an integrated MEMS sensor is studied and results are compared from both MEMS and piezoelectric sensors. A modal analysis is performed, using data from all available sensors. Comparing the frequency response functions and the natural frequencies shows the limitations of the MEMS sensor. One can then correct the MEMS measurements, by using global statistical parameters calculated on the data or by defining a "filter" function between the signals, thus improving the signal-to-noise ratio. It is found that MEMS sensors may replace piezoelectric ones for diagnostic applications. This way, an inexpensive measurement system (which needs to be calibrated only once, before installation, against higher-accuracy sensors) can be used for vibration monitoring of electric motors.

1 Introduction

In *condition monitoring*, one aims to diagnose potential faults in a machine or a component, by measuring and analizing relevant parameters during operation. Commonly, vibration analysis is employed for this goal, as vibration signals allow the specialist to diagnose a fault well in advance of a possible catastrophic failure. Moreover, advanced signal processing tools can be applied to analyze the vibration data and provide a detailed diagnosis, not just of the presence of a fault, but also of the components which are beginning to show damages.

Another powerful diagnostic tool using vibration measurements is *modal analysis*, to obtain the natural modes (and the corresponding natural frequencies) of a given mechanical system. Modal analysis, too, can be applied for maintenance monitoring, as cracks and wear can be detected by a change in the dynamic characteristics.

While both condition monitoring and modal analysis have found widespread use in several industries, a significant drawback that still limits even wider usage is the total cost of the required vibration measurement system, of which a significant share is generally due to the vibrations sensors. *Piezoelectric accelerometers* are most common in these applications, due to their accuracy and wide bandwidth; however, these are high-end instruments, usually with a cost in the hundreds of euros (as shown by manufacturers' catalogs). Also, they are relatively sensitive to violent shocks, which hinders applications in environments that require ruggedness.

In the last few decades, devices of a new type, namely *Micro Electro-Mechanical Systems* (MEMS)[1], have seen an explosive growth in industrial applications: these devices, which can be used either for sensing, actuation or control of mechanical variables, are defined as a whole by their small sizes[2]. Globally, MEMS now have a market of billions of euros, due to the general advantages of their batch micromanufacturing production process and, in particular, their low cost. Here, we are specifically interested in MEMS accelerometers: these sensors are used today in many everyday objects, such as airbag release systems in cars (one of their earliest applications) or IMU units in smartphones [1], and are now produced by the hundreds of millions per year.

[1] At times also equivalently called *"microsystems"* or *"micromachines"*; here we use the acronym MEMS, as it is more common.
[2] Strictly speaking in the order of micrometers, although the acronym is loosely used for systems up to a few millimeters in size.

MEMS accelerometers have attractive advantages for industrial vibration monitoring: besides their small size, cost (usually in the range of a few euros) and weight, they are also very rugged, again thanks to their small size. Thus, they can be integrated in hard-to-reach areas, even close to potential fault points, with minor effects on the measurements. Also, they have low energy requirements, so that they can be used for long-term monitoring within battery-powered systems that can work wirelessly for long periods without assistance [2]. Finally, MEMS accelerometers are often sold within off-the-shelf integrated circuits [3] with signal conditioning tools (such as ADC and signal amplifier) that allow the user to promptly integrate them in a measurement system. For reviews on the applications of MEMS accelerometers for vibration analysis, we refer the reader to [2, 4].

While already common for monitoring in civil engineering, MEMS vibrometers have so far received less attention for industrial environments. Admittedly, MEMS accelerometers have limited bandwidths with respect to standard piezoelectric ones, although MEMS have better low-frequency response and can even measure the static gravitational[3] acceleration [3]. The resolution and full-scale range of MEMS accelerometers are also generally lower. Finally, MEMS sensors have in general higher noise density levels (around 10-100 $\mu g/\sqrt{Hz}$).

Monitoring vibrations through MEMS has nevertheless been proposed in many fields, especially where remote application and long device life are crucial, for example in large-scale structures, such as airplane wings [5] and wind turbine blades [6]. MEMS devices have been applied to monitor the health of civil structures, such as bridges [7] or buildings, or to record earthquake data. Modal analyses of structures, such as shear frames [4, 8] or milling machines [8], have also been performed with MEMS devices. Finally, researchers have applied MEMS sensors for condition monitoring of diverse machines, such as air compressors [9], robotic arms [10], band saws [11], paper machines [12], CNC machines [13, 14], and hydraulic [15] and vacuum [16] pumps.

Rotating machines are a frequent target for condition monitoring; in particular, a large part of the total energy consumption in a factory is due to electric motors, thus their maintenance is of great importance. Several works [17–20] show how to detect vibrations on induction electric motors through MEMS devices; these can be inexpensively deployed in large numbers to remotely monitor machine fleets through industrial wireless sensor networks connected to a central maintenance analysis system, while guaranteeing very long autonomy times. Motor vibrations can be due to various types of faults, such as shaft misalignment, structural looseness, rotor [21] or electric [22] unbalance, or damages in the roller bearings [23]: such failures lead to easily recognized peaks in the vibration spectrum, that can be detected even with the higher noise levels that are typical of MEMS accelerometers. These sensors can even be applied directly on the shaft of rotating machines [24] or within a hollow rotor [25], to get as close as possible to the potential sources of vibrations and thus improve observability. Besides vibrations, current signals from motors can also be used for diagnosis [18, 20, 26]; MEMS current sensors may then be introduced, while integrating information from different signals [27].

In this paper, we study a prototype of an electric motor with an integrated MEMS sensor [28]. This motor is a variant (not yet released on the market, but currently under test at some customers of the manufacturer) of a commercial brushless motor commonly employed on automated machines; the role of the sensor is to measure the vibrations of the motor during operation. We show how to use the data from the MEMS to obtain the modal properties of the motor: these could be recorded in real-time and used to monitor the motor status during operation. Due to the limited performance of the MEMS accelerometer, especially in the wide bandwidth used for condition monitoring, we also use data from high-quality accelerometers attached on the outside of the motor. These accelerometers can be used to calibrate the MEMS, by finding a correlation between the vibration signals: while this procedure may be time-consuming, it need only be performed once, under laboratory conditions, while the results are specific for the motor under exam and can be reused at a later time.

The rest of this work is structured as follows. In Sec. 2, we present the motor under exam and the sensors used for the modal analysis. We also mention common sensing principles of MEMS accelerometers and summarize the dynamic model of the most common designs. In Sec. 3, we discuss the measurement setup, while in Sec. 4 we present the modal analysis results, namely the natural frequencies and the corresponding modes; these are derived using both the integrated MEMS sensor and external piezoelectric accelerometers, which are used as a reference (due to their higher accuracy). In Sec. 5, we analyze how the data from the different sensors are correlated; combining concepts from previous works in a novel way, we show that the MEMS signal can be filtered to compensate for the intrinsic limitations of this device. Finally, in Sec. 6 we present our conclusions and offer suggestions for future work.

[3] In the following, all accelerations are in units of gees (g), equal to the gravitational acceleration on Earth (1 g = 9.80665 m/s^2).

2 Motor and sensor design

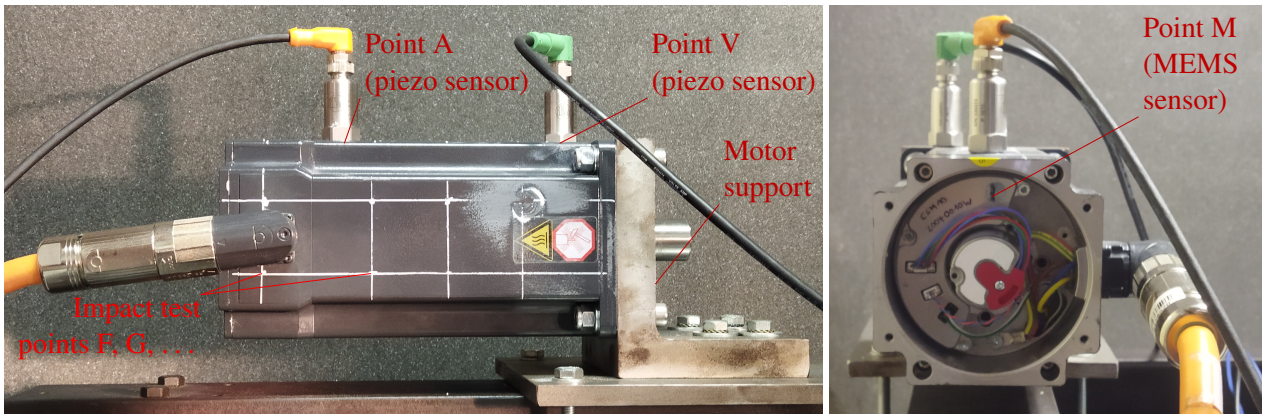

(a) (b)

Figure 1: The brushless synchronous motor under exam, in a front (a) and side (b) view, on our test bench.

We study a brushless synchronous electric motor, often used in automatic machines, shown in Fig. 1. While otherwise identical to a standard element of this series, this is in fact a prototype, soon to be released on the market, having an integrated, single-axis, capacitive MEMS accelerometer (model ADXL1002) by Analog Devices [28] attached to the rotor; see the side view (Fig. 1b), in which the back cover has been removed[4]. In Figs. 1a and 1b other accelerometers (glued on the motor cover) are also visible: these are high-quality, single-axis piezoelectric accelerometers (model VSP001) by ifm electronic [29]. The properties of the different accelerometers are compared in Tab. 1. As it can be seen, the MEMS sensor has significantly smaller size, weight and cost with respect to the piezoelectric one; the energy requirements are also reduced and the maximum (shock) admissible acceleration is larger. The bandwidth, which used to be much smaller in older MEMS models, is nowadays compatible with industrial monitoring requirements. The main limit of the MEMS is the noise level: for a bandwidth of 10000 Hz, the RMS noise level is $\left(25\ \mu g/\sqrt{\text{Hz}}\right)\left(\sqrt{10000\ \text{Hz}}\right) = 2.5$ mg [16], larger by an order of magnitude than the value for the piezoelectric sensor (assuming that no filter is used).

2.1 MEMS accelerometers

While a number of concepts have been proposed for inertial sensors [1, 3], most MEMS accelerometers apply either one of two main physical principles of operation, namely piezoelectric and capacitive (see Fig. 2).

Piezoelectric MEMS (Fig. 2a) generally employ a seismic mass suspended on a cantilever beam. A piezoelectric element attached on said beam measures its deformation, which is proportional to the applied load (namely, to the inertial force on the mass). The voltage generated by the piezoelectric element is thus proportional to the acceleration. Unlike conventional (non-MEMS) piezoelectric accelerometers, these sensors are not preloaded.

Capacitive MEMS (Fig. 2b), too, have a seismic mass connected to the fixed frame by flexible beams. Here, however, the displacement of the mass (proportional to the acceleration a) is measured by a variation in the capacitance between two sets of "fingers", some being attached on the mobile mass, while the others are on the frame. Consider, for simplicity, a single mobile finger and the two fixed fingers on its left- and right-hand side: the capacitances associated with the two finger pairs (on the left and on the right) are then equal to

$$C_L(0) = C_R(0) = \varepsilon\frac{A}{d} = C_0 \tag{1}$$

where ε is the dielectric permittivity, A is the area of overlap between the fingers, and d is the distance between each finger pair. After a displacement x (towards the left) of the mobile finger, the capacitances become

$$C_L(x) = \varepsilon\frac{A}{d-x}, \quad C_R(x) = \varepsilon\frac{A}{d+x} \tag{2}$$

[4]In this figure, irrelevant parts of the image have been covered, also due to non-disclosure agreements regarding the prototype.

Table 1: Comparison of the main properties for the two types of single-axis accelerometers (MEMS and piezoelectric) used in our tests. All technical data are from the manufacturers' catalogs [28, 29].

Property	**VSP001** (piezoelectric)	**ADXL1002** (MEMS)
Minimum frequency	2 Hz	0 Hz
Maximum frequency	10 kHz	11 kHz
Measuring range	± 50 g	± 50 g
Sensitivity	100 mV/g	40 mV/g
Shock resistance	5000 g	10000 g
Noise	0.1 mg	25 µg/$\sqrt{\text{Hz}}$
Cross axis sensitivity[a]	± 5%	± 1%
Typical operating voltage	10 V to 12 V	5 V
Typical current consumption	0.5 mA to 8 mA	1 mA
Admissible temperature range	-55 °C to +125 °C	-40 °C to +125 °C
Weight[b]	73.5 g	< 10 g
Maximum linear dimension[b]	46.5 mm	≃ 20 mm
Unit price[b,c]	≃ 240 €	≃ 80 €

[a] The cross axis (or transverse) sensitivity is defined as the maximum coupling between an excitation along an axis perpendicular to the axis of measurement and the measured signal.
[b] The values for the MEMS are relative to the evaluation board EVAL-ADXL1002Z on which it is mounted.
[c] The prices reported are those available from selected online resellers as of 2022-07-01.

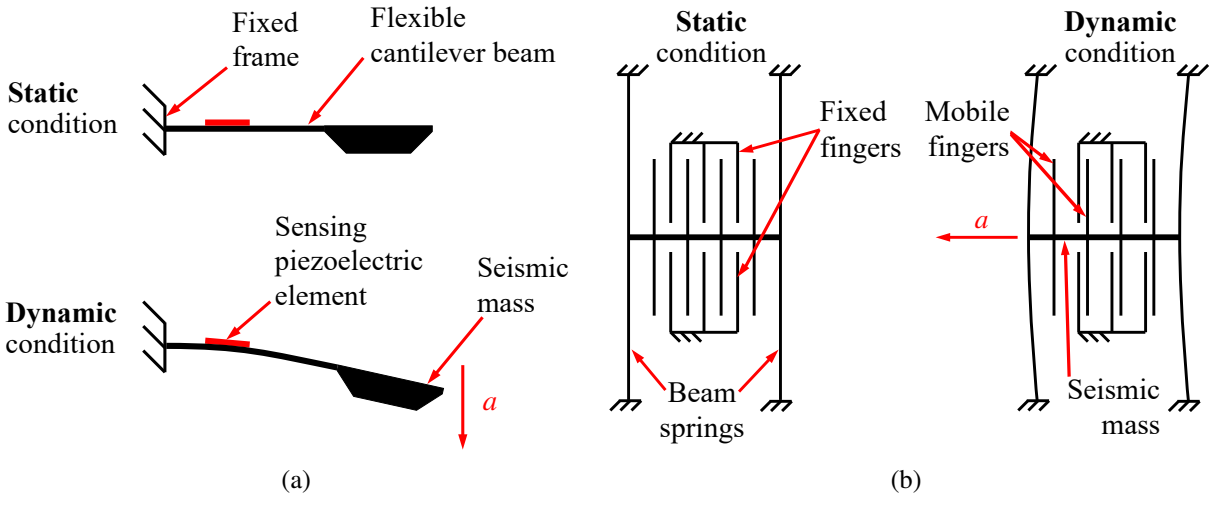

Figure 2: Schematics for the most common MEMS accelerometers: (a) piezoresistive, (b) capacitive.

In the assumption of small displacements, it can be shown that the displacement x is approximately given by

$$x \simeq \frac{d}{C_0} \frac{C_L(x) - C_R(x)}{2} \tag{3}$$

Similar results hold for the comb-like MEMS in Fig. 2b, with capacitances in parallel to increase the sensitivity.

Note that the concepts in Fig. 2 are not restricted to MEMS sensors (although they advantageously lend themselves to miniaturization) and can even measure *constant* accelerations, due to, for instance, gravity.

While both concepts shown in Fig. 2 have advantages and limitations, capacitive inertial sensors are currently dominant in the market, as they have generally lower noise floor levels, temperature sensitivity (but higher sensitivity to electromagnetic interference), power dissipation and drift, while providing higher measurement sensitivity. For these reasons, the MEMS sensor applied in the prototype (Fig. 1) is of the capacitive type.

3 Measurement setup

The measurement setup is shown in Fig. 1, where two piezoelectric accelerometers are mounted on the motor cover with cyanoacrilate glue. Adhesives are frequently applied for quickly mounting accelerometers, both MEMS and conventional piezoelectric ones [30], since they provide high stiffness and thus larger bandwidth, while allowing for quick removal. The MEMS sensor, on the other hand, is embedded in the motor itself, behind the "C" shaped cover in Fig. 1b (removing the cover, which protects the sensor, would risk damaging the sensor itself, therefore this cover has not been removed in the photos). The MEMS sensor is thus connected to the motor frame, albeit at a different position (close to the rotor) than the other piezoelectric accelerometers. The axis of measurement for all sensors is along the vertical direction, since the vibration signal (due to, for instance, bearing faults or rotor unbalance) is expected to be stronger in radial directions.

A force sensor, namely a impulse hammer, has also been introduced in our tests, to measure the excitation applied. Since the MEMS sensor is embedded in the motor design and cannot be easily removed, all the sensor channels have been recorded through the software interface of the industrial PC used to control the motor rotation: this PC is connected to the servo system that sends control signals to the motor, measures the encoder rotation and manages the power supply. The tests were performed in static conditions, to derive the modal properties when the system is at rest. This industrial prototype is designed to read data from the MEMS sensor during motor operation: the other channels of measurement (corresponding to the piezoelectric accelerometers and the hammer) are then recorded through add-on EtherCAT terminals that are connected to the PC. This way, we can either measure vibration and force signals in real time or record the data over a given period in .CSV format for later analysis. The channels are sampled at 16 kHz, which is well above the upper limit of the frequency ranges for the sensors (see Tab. 1); we thus added a low-pass filter in our study. The sensitivities of each sensor (known from previous calibrations) were also set in the industrial PC interface.

In the following, for conciseness, the results from the piezoelectric sensor on the left-hand side (the one with the orange connector in Fig. 1a) are denoted as "Piezo A", while the results from the sensor on the right-hand side (green connector) are denoted as "Piezo V", and the remaining channels are "Hammer" and "MEMS". The attachment points of the accelerometers correspond to points A and V in the schematic in Fig. 3, while point M roughly corresponds to the projection (on the left view plane) of the position of the MEMS sensor, which is not visible in Fig. 3. All the other points in the schematic, namely B–L, N–U and W, correspond to the reference points for measurements, on which an impact force has been applied through the hammer; the figure also reports the coordinates of said points (all dimensions in mm), together with the reference coordinate frame. Eight other points, named Bn to In, were also used; these points are not shown in the figure, for brevity, since they are defined by the same coordinates as points B to I, respectively (but on the opposite face with respect to the one in the front view). Five impact tests were repeated for each point, to reduce the noise levels by averaging the results. All data were saved and later analyzed in MATLAB, for convenience; the integrated software for the industrial PC does not include algorithms for spectral data analysis yet.

4 Frequency response analysis

Example data from one test (on point G in Fig. 3) are presented in Fig. 4: the data from the three accelerometer channels (one MEMS and two piezoelectric sensors) are in Fig. 4a, while Fig. 4c displays the corresponding readings for the impulse hammer. Only a segment of the total recording time (5 s) is shown, corresponding to

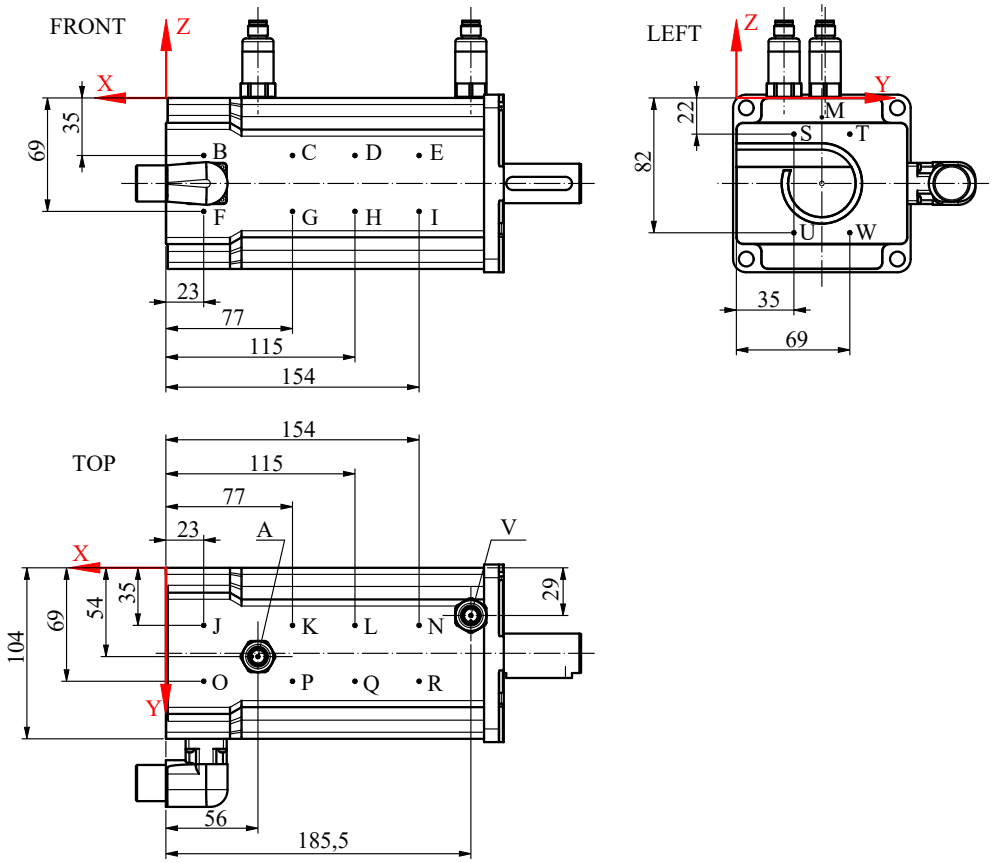

Figure 3: Schematic of the motor, with the measurement and excitation points and the XYZ coordinate frame.

the period immediately after the impact. From Fig. 4, it is apparent that the MEMS sensor can record the vibration as it dissipates, but has relatively high levels of noise when compared to the piezoelectric sensors.

The corresponding power spectra are in Figs. 4b and 4d, respectively for the acceleration and for the force data. We restricted the frequency range to $[0\ \text{Hz},\ 1700\ \text{Hz}]$, as outside this range the input force power spectrum drops off too abruptly (Fig. 4d). As shown in Fig. 4b, some spectral peaks are clearly visible for both piezoelectric accelerometers; those same peaks are also present in the spectrum of the MEMS signal, although less recognizable due to the limits of the sensor. This suggests that we should be able to detect at least some of the natural frequencies of vibration and of the corresponding modes of the motor (and of the structure to which it is fixed) from the MEMS data, but some calibration may be needed to increase the signal-to-noise ratio.

4.1 Identification of natural frequencies

For each of the 28 excitation points in total, one can define a *Frequency Response Function* (FRF) from the excitation to the measurement point, which can be either A, V or M, corresponding to the three accelerometers (see again Fig. 3). Using again the data from the tests on point G as an example, the plots of the magnitudes of the three FRFs (one for each accelerometer) are shown in Fig. 5; all plots shown are functions of the frequency on the x axis. These values are actually obtained by averaging five FRFs plots, one for each repetition of the test, as discussed in Sec. 3.

In Fig. 5, we also report the stabilization diagrams for each set of FRFs; the natural frequencies thus found are shown with different markers, depending on whether their values (and the values of the corresponding modal damping ratios) are stable when the modal order is increased. A maximum number of 22 modes has been chosen for the analysis. As it can be seen from the figure, the accelerometers signals have different FRFs (with respect to the input force) and thus different stabilization diagrams; this is indeed to be expected, not just due to the different properties of the sensors, but also because the sensor positions on the motor are different.

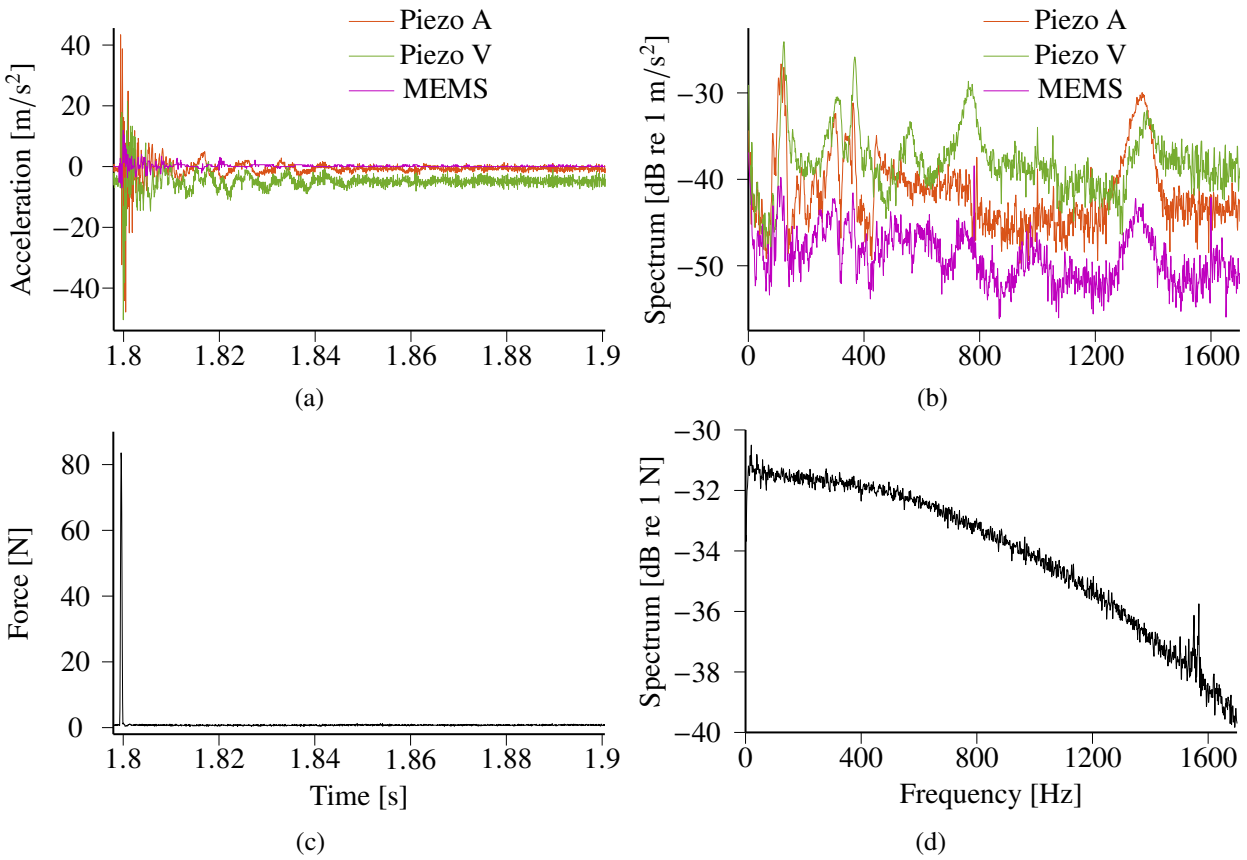

Figure 4: Data from a test: accelerometer and hammer readings (Figs. a and c) and their spectra (b and d).

Table 2: List of the first six stable detected frequencies of vibration for the motor structure: for each column, the results of the stabilization diagram for the corresponding sensor are reported, using data from tests on all excitation points. Only the data from stable modes with coherence above 0.75 are reported.

Stable mode n.	**Stable frequency from piezo A** [Hz]	**Stable frequency from piezo V** [Hz]	**Stable frequency from MEMS** [Hz]	**Stable frequency from SCADAS** [Hz]
1	117.4	120.4	118.2	123.0
2	303	309	300	314
3	362	369	358	359
4	442	449	444	443
5	778	779	776	780
6	1376	1384	1378	1375

However, some frequency peaks are common between the three FRFs and correspond to modes that are stable (at least in terms of their frequencies); the most prominent, for instance, are those around 118 Hz and 1380 Hz. Since these also correspond to relatively high values of the coherence γ (>0.75 for all three sensors), these seem to correspond to actual natural frequencies of the motor, including the structure to whom it is attached. Other frequency peaks, however, are less visible: for instance, a stable mode at about 770 Hz is clearly detected by the piezoelectric sensors, but no corresponding mode is found by the MEMS sensor at the same frequency. For these reasons, the modal frequencies were re-derived using data from all tests, namely averaging the FRFs

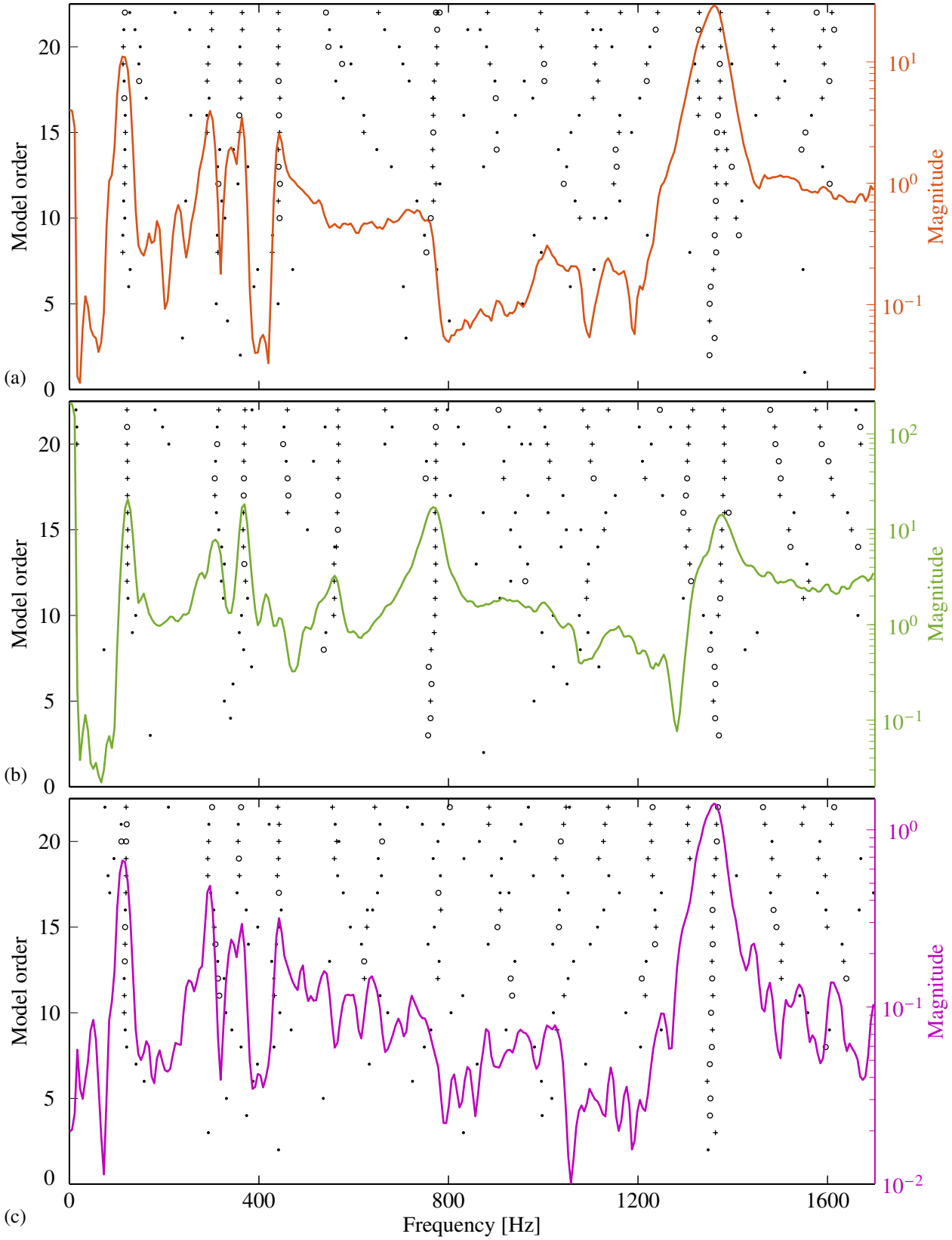

Figure 5: Data from the tests with excitation on point G: stabilization diagrams for the average FRFs, relative to the sensors in points A (a), V (b) and M (c). In these diagrams, the dots correspond to poles that do not remain stable between consecutive modal orders, the circles to poles that are stable in frequency (but not in damping), and the crosses to poles that are stable in both frequency and damping; the modal order is shown in the scale on the left, while the FRF magnitude is in the (logarithmic) scale on the right.

from all excitation points and all repetitions of each test; the corresponding global stabilization diagrams are not reported here, for brevity. The natural frequencies of the first six modes, that are common between all three sensors, are reported in Tab. 2: as it can be seen, the results are approximately equal, since the frequencies differ by less than 5 %. This suggests that the data from the MEMS sensor are indeed reliable enough for further analysis.

We also performed a second set of tests, whose setup is not shown here, for brevity; in this case, however, we did not use the industrial drive seen so far to record the force and acceleration data. Instead, we used a Simcenter SCADAS Mobile acquisition hardware, connected to high-accuracy piezoelectric accelerometers from our laboratory: since these are significantly smaller than the industrial sensor VSP001 previously mentioned (while offering comparable performances in terms of noise levels and frequency ranges), we can apply more accelerometers without substantially altering the modal parameters of the motor and its structure. In this case, seven accelerometers were glued on the external body of the motor; of these, four are triaxial and the remaining ones monoaxial, for a total of 15 acceleration channels. Therefore, unlike the previous tests, we have excitation channels along all the three coordinate axes shown in Fig. 3; this way, an accurate description of the modal shapes may be obtained. The structure vibration was excited manually, with the same impulse hammer used in the previous set of tests. This second set of experiments does not include data from the MEMS sensor, but is instead used as a reference against which the modal analysis from the industrial drive can be compared. The results were then analyzed through Test.Lab software, to derive "reference" FRFs and the corresponding modal stabilization diagrams. Again, it was found that the stable frequencies thus obtained were in good agreement with those found using the MEMS sensor; these results, too, are shown in Tab. 2.

5 Filtering the MEMS data

As shown previously, the MEMS sensor can detect the motor vibration, but the signal has a relatively high noise level. One then needs to correct for the limitations of this sensor: indeed, it is known that MEMS devices, being mass-produced, can have high variability in their main parameters with respect to the reference values on their catalogs. The most immediate option would be to perform an experimental characterization of the sensor, for instance on a shaker table, to accurately calibrate its main parameters, such as sensitivity, linearity and frequency response [31], by applying known excitations, such as random noise or a sinuisoidal excitation [14, 32]. This, however, would require a controlled environment, due to the temperature sensitivity of the sensor and the need to isolate it from background noise; this would be even less convenient in our case, since the sensor is already embedded in the motor. Even then, the results would be still relatively noisy.

Another possibility is to compare the results from the MEMS sensor with those from a more accurate accelerometer mounted close to it: this way, the effect of the structure on which the sensors are mounted is minimized, and the signal vibration should be identical (up to the difference in sensitivities and noise levels). The goal is then to correlate the two different signals, such that the signal of the piezoelectric sensor can be reconstructed from the MEMS signal. The simplest approach would be to find global statistical coefficients to be corrected, for instance from a linear-least-squares correlation on the signals: the data from the piezoelectric channel could then be estimated from a linear transformation of the data from the MEMS sensor. In our tests, however, this approach proved unfruitful. A more interesting option is to compare the spectral data from the two channels: this way, one can derive an FRF, not between a vibration sensor and a force sensor, as it is usually done in experimental modal analysis, but between two accelerometers [14, 32]. In particular, some authors [33] have considered optimal filters defined from such a FRF: several numerical algorithms are known from the literature (and available, for instance, as MATLAB routines) to derive the parameters of a filter, with given numbers of poles and zeros, providing the best approximation to a target FRF.

This filter could be derived, for instance, by comparing the spectra shown in Fig. 4b relative to the MEMS and to the other two sensors. However, in this way the filter would include effects due not only to the intrinsic differences in the sensors, but also to the fact that the MEMS is measuring at a different position. To properly calibrate the filter which approximates a piezoelectric sensor from the data of the MEMS filter, we then need to measure comparable accelerations in the same point. While other authors [33] tuned their filter from tests on a separate test bench, including only the sensors of interest, we found it more effective and practical to record

data directly on the motor. This way, our results are targeted for the specific sensor in use: this is desirable to obtain better accuracy, since MEMS sensors have relevant variations with respect to their standard parameters (as reported by catalogs). We then performed another set of tests, in which a triaxial piezoelectric sensor was glued on the metal cover shown in Fig. 1b, as close as possible to the MEMS position; a set of five tests was repeated with the back cover of the motor removed, to connect the triaxial accelerometer to the industrial drive for recording. Note that removing the back cover alters the modal analysis of the entire structure, but in this case we are only interested in the comparison between the sensors. This way, the results will depend almost entirely on the differences between sensors. The channel of the triaxial sensor corresponding to the vertical direction was compared with the MEMS data, since the axis of measurement of this sensor is also along the same direction; the data from the other two axis of the triaxial sensor were found to be less correlated and were thus ignored in further analyses. Again, we excited vibrations on the motor structure with the impulse hammer, acting as close as possible to the sensors under comparison and hitting along the vertical direction, to obtain more significant results. The force data was also recorded, but was found to be not useful in this analysis, since we are interested only in the FRF between the two accelerometric sensors.

The data was then analyzed with the System Identification Toolbox available in MATLAB. We only took into account the relevant parts of the measured signals, namely for 3 ms before the impact and 125 ms after the impact: the recorded data over time are shown in Fig. 6b for the piezoelectric sensor. From these data, we computed the power spectra shown in Fig. 6a: while some peaks[5] are common between the two sensors (compare the red and the green lines), it is clear that the results from the MEMS are not equivalent to those from a more accurate sensor, thus we need to improve the results. We then considered only the frequency range between 0 and 1700 Hz; to each signal, we subtracted its average value, which is not relevant for this analysis (in any case, a constant offset between the sensors can be easily corrected after filtering). The spectra were also normalized by setting the maximum value for each of them to one: this is necessary to compare the spectra from the piezoelectric sensor and from the (unfiltered) MEMS sensor, since the latter has much lower levels of energy. This scaling can be easily taken into account later, by introducing a constant gain.

We applied a linear, discrete-time filter of order 10 fitted over the spectra; the degree of the filter was found by trial-and-error, with the goals of obtaining an acceptable fit between the different spectra while avoiding overfitting. This latter issue was checked by applying the filter derived for a particular test over different repetitions of the same test. The transfer function of the filter, in the z-domain, is defined by

$$H(z) = \frac{\sum_{i=0}^{10} b_i z^{-i}}{1 + \sum_{i=1}^{10} a_i z^{-i}} \tag{4}$$

where the (constant) polynomial coefficients a_i and b_i are reported in Tab. 3. With these definitions, the filter is found to be *stable*, meaning that the impulse response decays to zero: indeed, as shown in Fig. 7a, all its poles are within the unit circle in the complex z plane [33]. Moreover, our filter is *causal*, since its output at any given time only depends on current and previous input values: this is guaranteed by the fact that the numerator and the denominator in Eq. (4) are defined by polynomials of the same degree. These two conditions guarantee that the filter is *realizable*, namely, that it can be realized as a digital-filter network. The frequency behavior of this filter, in terms of its phase and amplitude response, are shown in Fig. 7b. Finally, applying the filter to the original MEMS sensor data, we obtain the results in the plot shown in Fig. 6a (over

Table 3: List of the coefficients for the polynomials in the discrete-time filter from Eq. (4).

i	0	1	2	3	4	5	6	7	8	9	10
b_i	292	−2650	11000	−27400	45700	−52900	43200	−24600	9310	−2120	221
a_i	—	−9.11	37.9	−95.2	159.4	−185.7	152.7	−87.4	33.4	−7.67	0.807

[5]Note that these frequency peaks are *not* the same as those seen previously, which were mostly due to the structure of the motor.

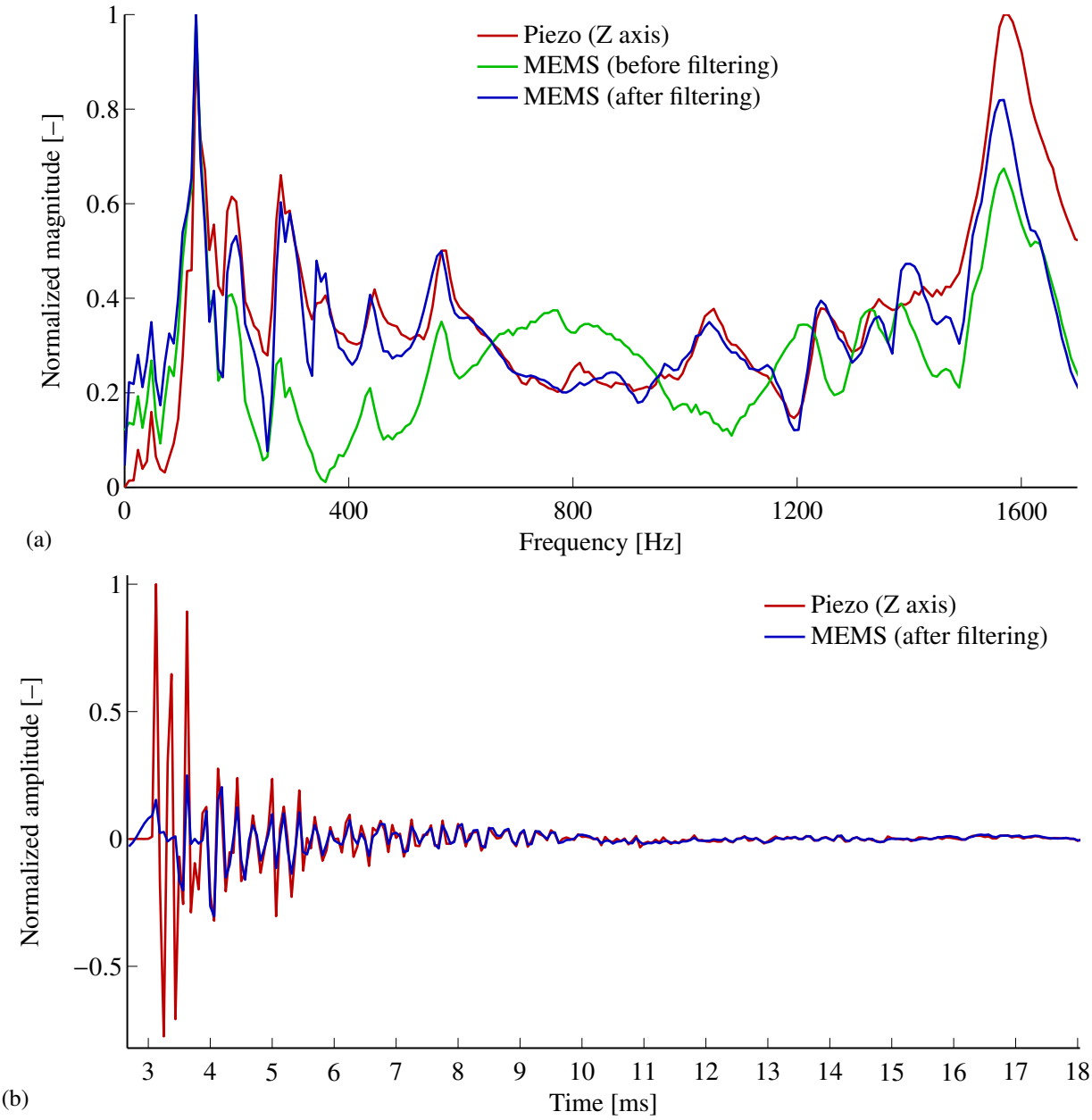

Figure 6: Comparison of the data from the Z (vertical) axis of the piezoelectric sensor (in red line) with the data from the MEMS sensor, before (in green) and after applying our filter (in blue): the plots show the results in the frequency domain (a), where the filter is defined by comparing the spectra, and in the time domain (b).

the frequency domain): it can be seen that, after filtering, the spectral data of the MEMS sensor is reasonably close to those from the piezoelectric sensor. The signals were also compared in the time domain (Fig. 6b): here, too, we normalized the maximum values to one, to show the measured vibrations over time.

6 Conclusions

Integrating low-cost MEMS accelerometers in the design of servo motors has been suggested for some time [34] to expand the possibilities of condition monitoring in industrial environments. In this work, we have tested a prototype of a servo motor for automatic machines, which includes a MEMS accelerometer integrated in the design: this sensor sends the measured data to the industrial PC used to control the motor.

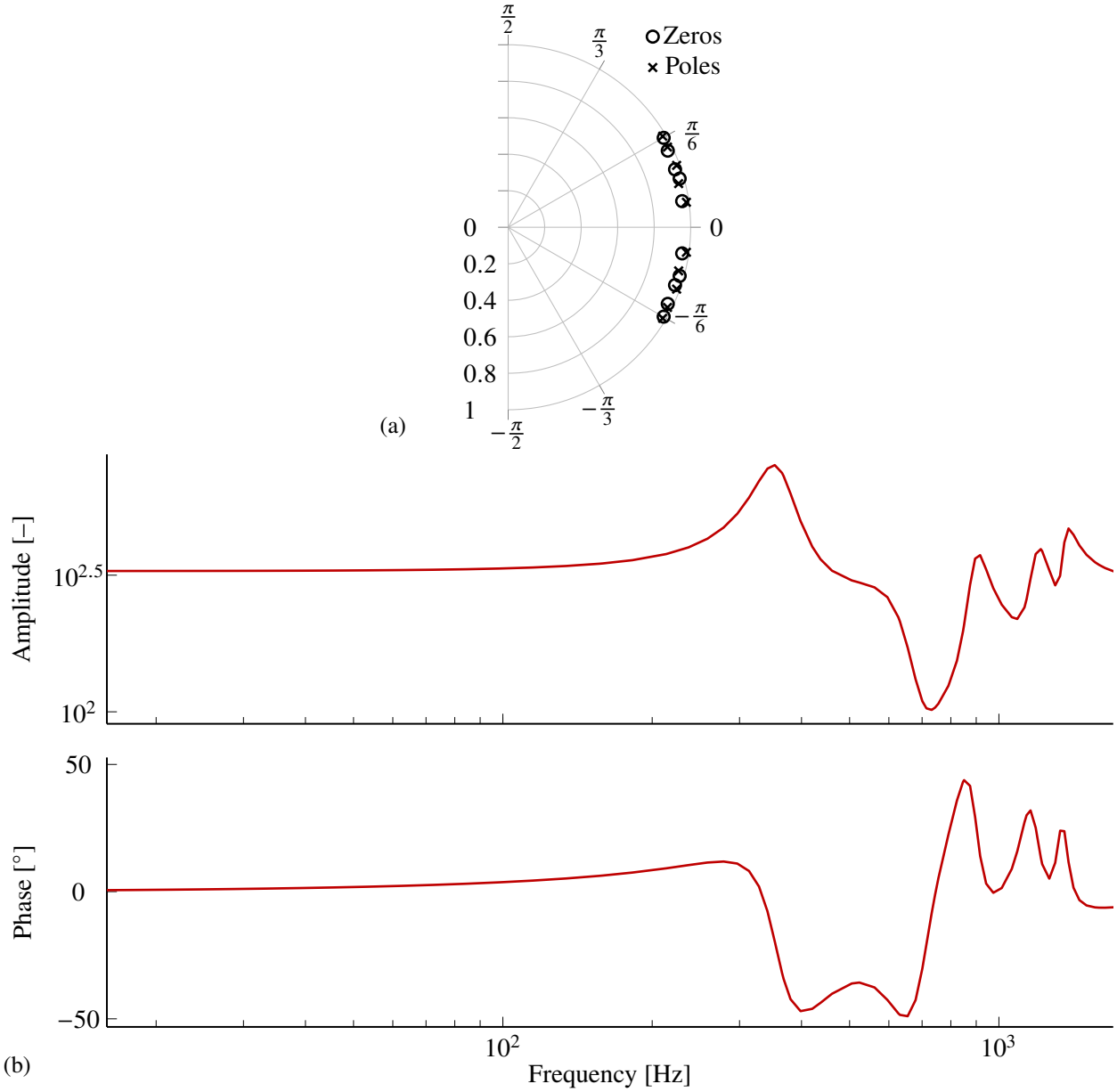

Figure 7: Properties of the filter defined between the MEMS and the piezoelectric sensor data: in (a), the poles and the zeros (denoted as crosses and circles, respectively) are shown in the complex plane, while in (b), the filter response is plotted (in logarithmic scale) over the frequency range of interest.

This way, real-time vibration data can be used to diagnose the status of the motor, by detecting frequency peaks corresponding to faults in the motor components (such as the rotor and the bearings). First, however, one needs to know the modal properties of a "healthy" motor where faults have yet to occur, to be used as a reference for condition monitoring analysis. Moreover, we also needed to verify whether the MEMS sensor applied has indeed the required accuracy for practical use in this field; while MEMS accelerometers have generally been perceived as excessively noisy for machine diagnostics, their continuous development makes them increasingly attractive over standard piezoelectric sensors.

The aim of our research is to calibrate a condition monitoring device as a MEMS sensor system embedded in the motor itself and connected to the industrial PC already used for motion control. In industrial applications, this system will no longer require the external piezoelectric accelerometers, which are more expensive and less rugged. In tests currently underway at our laboratory, we are using this device to detect characteristic frequencies on faulty bearings: while some preliminary results have already been obtained, it is first necessary

to understand how the MEMS signal may be improved for better detection capabilities and to define the natural frequencies of the motor itself, regardless of the mechanism which it actuates. In this sense, this work is a stepping stone towards a complete, MEMS-based condition monitoring system.

References

[1] V. Kempe, *Inertial MEMS: principles and practice*. Cambridge University Press, 2011. doi:10.1017/CBO9780511933899.

[2] A. Sabato, C. Niezrecki, and G. Fortino, "Wireless MEMS-based accelerometer sensor boards for structural vibration monitoring: a review," *IEEE Sens. J.*, vol. 17, no. 2, pp. 226–235, 2017, doi:10.1109/JSEN.2016.2630008.

[3] D. K. Shaeffer, "MEMS inertial sensors: a tutorial overview," *IEEE Commun. Mag.*, vol. 51, no. 4, pp. 100–109, 2013, doi:10.1109/MCOM.2013.6495768.

[4] M. Varanis, A. Silva, A. Mereles, and R. Pederiva, "MEMS accelerometers for mechanical vibrations analysis: a comprehensive review with applications," *Journal of the Brazilian Society of Mechanical Sciences and Engineering*, vol. 40, p. 527, 2018, doi:10.1007/s40430-018-1445-5.

[5] C. Ratcliffe, D. Heider, R. Crane, C. Krauthauser, M. K. Yoon, and J. W. Gillespie, "Investigation into the use of low cost MEMS accelerometers for vibration based damage detection," *Compos. Struct.*, vol. 82, no. 1, pp. 61–70, 2008, doi:10.1016/j.compstruct.2006.11.012.

[6] O. O. Esu, S. D. Lloyd, J. A. Flint, and S. Watson, "Feasibility of a fully autonomous wireless monitoring system for a wind turbine blade," *Renew. Energy*, vol. 97, pp. 89–96, 2016, doi:10.1016/j.renene.2016.05.021.

[7] C. Bedon, E. Bergamo, M. Izzi, and S. Noè, "Prototyping and validation of MEMS accelerometers for structural health monitoring—The case study of the Pietratagliata cable-stayed bridge," *J. Sens. Actuator Netw.*, vol. 7, no. 3, p. 30, 2018, doi:10.3390/jsan7030030.

[8] Y. J. Chan and J.-W. Huang, "Multiple-point vibration testing with micro-electromechanical accelerometers and micro-controller unit," *Mechatronics*, vol. 44, pp. 84–93, 2017, doi:10.1016/j.mechatronics.2017.04.006.

[9] G. Feng, N. Hu, Z. Mones, F. Gu, and A. D. Ball, "An investigation of the orthogonal outputs from an on-rotor MEMS accelerometer for reciprocating compressor condition monitoring," *Mech. Syst. Signal Process.*, vol. 76–77, pp. 228–241, 2016, doi:10.1016/j.ymssp.2015.12.033.

[10] A. A. Jaber and R. Bicker, "Design of a wireless sensor node for vibration monitoring of industrial machinery," *Int. J. Electr. Comput. Eng. Syst.*, vol. 6, no. 2, pp. 639–653, 2016, doi:10.11591/ijece.v6i2.9296.

[11] M. Magno *et al.*, "SmarTEG: an autonomous wireless sensor node for high accuracy accelerometer-based monitoring," *Sensors*, vol. 19, no. 12, p. 2747, 2019, doi:10.3390/s19122747.

[12] I. Koene, R. Viitala, and P. Kuosmanen, "Internet of things based monitoring of large rotor vibration with a microelectromechanical systems accelerometer," *IEEE Access*, vol. 7, pp. 92 210–92 219, 2019, doi:10.1109/ACCESS.2019.2927793.

[13] K. K. Tan, S. Huang, Y. Zhang, and T. H. Lee, "Distributed fault detection in industrial system based on sensor wireless network," *Comput. Stand. Interfaces*, vol. 31, no. 3, pp. 573–578, 2009, doi:10.1016/j.csi.2008.03.024.

[14] A. Albarbar, S. Mekid, A. Starr, and R. Pietruszkiewicz, "Suitability of MEMS accelerometers for condition monitoring: an experimental study," *Sensors*, vol. 8, no. 2, pp. 784–799, 2008, doi:10.3390/s8020784.

[15] Q. Hu, E. Firmeza Ohata, F. H. S. Silva, G. L. Bezerra Ramalho, T. Han, and P. P. Rebouças Filho, "A new online approach for classification of pumps vibration patterns based on intelligent IoT system," *Measurement*, vol. 151, p. 107138, 2020, doi:10.1016/j.measurement.2019.107138.

[16] S. Thanagasundram and F. S. Schlindwein, "Comparison of integrated micro-electrical-mechanical system and piezoelectric accelerometers for machine condition monitoring," *Proc. Inst. Mech. Eng., Part C*, vol. 220, no. 8, pp. 1135–1146, 2006, doi:10.1243/09544062C07405.

[17] S. Korkua, H. Jain, W.-J. Lee, and C. Kwan, "Wireless health monitoring system for vibration detection of induction motors," in *Proc. of the 2010 IEEE Ind. Commer. Power Syst. Tech. Conf.* Tallahassee, USA: IEEE, Jun. 2010, pp. 1–6, doi:10.1109/ICPS.2010.5489899.

[18] L. Hou and N. W. Bergmann, "Novel industrial wireless sensor networks for machine condition monitoring and fault diagnosis," *IEEE Trans. Instrum. Meas.*, vol. 61, no. 10, pp. 2787–2798, 2012, doi:10.1109/TIM.2012.2200817.

[19] B. Bengherbia, M. O. Zmirli, A. Toubal, and A. Guessoum, "FPGA-based wireless sensor nodes for vibration monitoring system and fault diagnosis," *Measurement*, vol. 101, pp. 81–92, 2017, doi:10.1016/j.measurement.2017.01.022.

[20] J. Medina-García, T. Sánchez-Rodríguez, J. A. G. Galán, A. Delgado, F. Gómez-Bravo, and R. Jiménez, "A wireless sensor system for real-time monitoring and fault detection of motor arrays," *Sensors*, vol. 17, no. 3, p. 469, 2017, doi:10.3390/s17030469.

[21] L. Agnoletti Dos Santos Pedotti, R. Mazza Zago, and F. Fruett, "Fault diagnostics in rotary machines through spectral vibration analysis using low-cost MEMS devices," *IEEE Instrum. Meas. Mag.*, vol. 20, no. 6, pp. 39–44, 2017, doi:10.1109/MIM.2017.8121950.

[22] S. B. Chaudhury, M. Sengupta, and K. Mukherjee, "Vibration monitoring of rotating machines using MEMS accelerometer," *Int. J. Sci. Eng. Res.*, vol. 2, no. 9, pp. 5–11, 2014. [Online]. Available: https://www.ijser.in/archives/v2i9/SjIwMTMzNTg=.pdf

[23] G. S. Maruthi and V. Hegde, "Application of MEMS accelerometer for detection and diagnosis of multiple faults in the roller element bearings of three phase induction motor," *IEEE Sens. J.*, vol. 16, no. 1, pp. 145–152, 2016, doi:10.1109/JSEN.2015.2476561.

[24] M. E. Elnady, J. K. Sinha, and S. O. Oyadiji, "Identification of critical speeds of rotating machines using on-shaft wireless vibration measurement," in *25th Int. Congr. on Cond. Monit. Diagn. Eng.* Huddersfield, UK: IOP Publishing, Jun. 2012, vol. 364, p. 012142, doi:10.1088/1742-6596/364/1/012142.

[25] S. Jiménez, M. O. T. Cole, and P. S. Keogh, "Vibration sensing in smart machine rotors using internal MEMS accelerometers," *J. Sound Vib.*, vol. 377, pp. 58–75, 2016, doi:10.1016/j.jsv.2016.05.014.

[26] G. Curcurù, M. Cocconcelli, F. Immovilli, and R. Rubini, "On the detection of distributed roughness on ball bearings via stator current energy: experimental results," *Diagnostyka*, vol. 3, no. 51, pp. 17–21, 2009. [Online]. Available: https://yadda.icm.edu.pl/baztech/element/bwmeta1.element.baztech-article-BAR0-0044-0003

[27] J.-D. Son, B.-H. Ahn, J.-M. Ha, and B.-K. Choi, "An availability of MEMS-based accelerometers and current sensors in machinery fault diagnosis," *Measurement*, vol. 94, pp. 680–691, 2016, doi:10.1016/j.measurement.2016.08.035.

[28] Analog Devices, "Low noise, high frequency MEMS accelerometers - Data sheet ADXL1001/ADXL1002," 2017. [Online]. Available: https://www.analog.com/media/en/technical-documentation/data-sheets/ADXL1001-1002.pdf

[29] ifm electronic GmbH, "VSP001 accelerometer - vibration sensor," 2015. [Online]. Available: https://www.ifm.com/ie/en/search?query=vsp001

[30] M. Cocconcelli and A. Spaggiari, “Mounting of accelerometers with structural adhesives: experimental characterization of the dynamic response,” *J. Adhes.*, vol. 93, no. 8, pp. 585–598, 2017, doi:10.1080/00218464.2015.1120197.

[31] C. Acar and A. M. Shkel, “Experimental evaluation and comparative analysis of commercial variable-capacitance MEMS accelerometers,” *J. Micromech. Microeng.*, vol. 13, no. 5, pp. 634–645, 2003, doi:10.1088/0960-1317/13/5/315.

[32] A. Albarbar, A. E. Badri, J. K. Sinha, and A. G. Starr, “Performance evaluation of MEMS accelerometers,” *Measurement*, vol. 42, no. 5, pp. 790–795, 2009, doi:10.1016/j.measurement.2008.12.002.

[33] A. E. Badri, J. K. Sinha, and A. Albarbar, “A typical filter design to improve the measured signals from MEMS accelerometer,” *Measurement*, vol. 43, no. 10, pp. 1425–1430, 2010, doi:10.1016/j.measurement.2010.08.011.

[34] D. Borghi and M. Cocconcelli, “Future challenges in condition monitoring from an industrial perspective: the case of the independent carts systems,” *Acoust. Aust.*, vol. 49, pp. 259–263, 2021, doi:10.1007/s40857-021-00225-6.